

Explainable Deep Learning for Augmentation of sRNA Expression Profiles

Jelena Fiosina^a, Maksims Fiosins^{b,c,d}, Stefan Bonn^{b,c}

^a*Clausthal University of Technology, Clausthal-Zellerfeld*

^b*German Center for Neurodegenerative Diseases, Tübingen*

^c*Institute for Medical Systems Biology, University Medical Center Hamburg-Eppendorf, Hamburg*

^d*Genevention GmbH, Göttingen, Germany*

Abstract

The lack of well-structured metadata annotations complicates the re-usability and interpretation of the growing amount of publicly available RNA expression data. The machine learning-based prediction of metadata (data augmentation) can considerably improve the quality of expression data annotation. In this study, we systematically benchmark deep learning (DL) and random forest (RF)-based metadata augmentation of tissue, age, and sex using small RNA (sRNA) expression profiles. We use 4243 annotated sRNA-Seq samples from the small RNA expression atlas (SEA) database to train and test the augmentation performance. In general, the DL machine learner outperforms the RF method in almost all tested cases. The average cross-validated prediction accuracy of the DL algorithm for tissues is 96.5%, for sex is 77%, and for age is 77.2%. The average tissue prediction accuracy for a completely new dataset is 83.1% (DL) and 80.8% (RF). To understand which sRNAs influence DL predictions, we employ backpropagation-based feature importance scores using the DeepLIFT method, which enable us to obtain information on biological relevance of sRNAs.

Keywords: augmentation, classification, deep learning, explainable artificial intelligence, random forest, ontology, small RNA expression, contamination

1. Introduction

Data annotations (tissue, age, sex, etc.) are crucial for the re-use of data. A detailed description of the biological conditions in which data has been obtained is required to extract new information from the obtained data. The data should be findable, accessible, interoperable, and reusable, which ultimately facilitates knowledge discovery (Wilkinson et al., 2016). Annotations are an essential part of semantic data integration systems and allow for a deeper analysis of the data (Madan et al., 2018). So far, metadata is often not stored together with the expression data and the available metadata is often not normalized, and is unstructured and incomplete. The widely used GEO repository (GEO), for example, stores annotations as a number of free-text description fields. This leads to missing and/or inaccurate annotations and requires revisions and manual corrections by an expert (Hadley et al., 2017). In this study, we aim to predict the metadata based on deep-sequenced small RNAs' (sRNAs') expression profiles by formulating this prediction

as a classification problem. sRNAs are short (less than 200 nt), usually non-coding RNA molecules with many crucial biological functions (Storz, 2002). The basic rationale for this approach is that data with similar sRNA expressions should have similar metadata. Based on this assumption, we hypothesize that sRNA expression profiles contain enough information to predict the sRNA tissue, age, and sex accurately. We believe that deep learning (DL)-based algorithms might outperform more conventional random forest (RF)-based machine learners (MLs) in sRNA metadata prediction, if enough training data is available. We also hypothesize that backpropagation-based feature importance scores may help to biologically rationalize the classification process of DL.

To distinguish between biological conditions, different ML methods were applied. In (Guo et al., 2017) and (Hadley et al., 2017), the sex in different micro RNA (miRNA) tissue samples was defined using differential expression (DE) analysis. In (Hadley et al., 2017), the authors used DE analysis and analysis of variance to detect the sex differences in several tissues in miRNAs. In (Ellis et al., 2018), the age, sex, and tissue were predicted from mRNA sequencing (mRNA-Seq) expression data using a regression-based approach. massiR (Buckberry et al., 2014) is a method for sex prediction based on gene expression microarrays using clustering. Many studies use an RF method for the classification of expression data, particularly in disease diagnostics (Statnikov et al., 2008). (Johnson et al., 2018) provides a good overview of ML methods for expression data analysis.

For our analysis, we used data from the sRNA expression atlas (SEA, <http://sea.ims.bio>) (Rahman et al., 2017), a database containing well-structured, manually curated, ontology-based annotations of publicly available sRNA-Seq data. All data from the SEA was analyzed with the same workflow (OASIS (Rahman et al., 2018), <https://oasis.dzne.de>). We used 4243 annotated human sRNA-Seq samples from the SEA.

We applied the DL and RF classifiers for the considered augmentation problem and compared their results. The RF classifier is an ensemble-based classifier, which outperforms other conventional classifiers for very high-dimensional data (Breiman, 2001). An RF classifier requires lesser training data in comparison with the DL classifier and allows the interpretation of features by generating variable importances. However, the RF classifier is sensitive to class imbalance (OBrien and Ishwaran, 2019).

DL is able to analyze big data and is robust enough to treat large amounts of noisy training data (LeCun et al., 2015), (Xiao et al., 2015). Its disadvantage is that, it requires large amounts of training data (Li et al., 2019), is prone to overfit for small training sets and is difficult to biologically interpret (feature importance) (Webb, 2018). In (Kong and Yu, 2018) the RF and DL approaches were used in two stages. For the first stage, the RF approach was used to extract the most important features and then for the second stage, the DL approach was implemented for gene expression data classification based on the selected features. Many researchers are currently trying to explain DL models (Bach et al., 2015), (Montavon et al., 2017), (Choi et al., 2016). Some methods are model-agnostic, which can explain the behavior of every "black box" or "grey box" model: (Lakkaraju et al., 2017), (Ribeiro et al., 2016), (Molnar, 2019). Some methods

are model specific, such as perturbation-based (Robnik-ikonja and Bohanec, 2018) or backpropagation-based (Shrikumar et al., 2017) models. We have used DeepLIFT (Shrikumar et al., 2017) scores to explain DL models.

In this study, we present that DL algorithms outperform RF-based data augmentation for tissue, sex, and age annotations using sRNA expression profiles, if enough training data is available. More specifically, the DL method performs better than the RF method for cross-validation experiments as well as on "one dataset out" experiments. We have demonstrated how backpropagation can provide a biological interpretation of relevant features for the DL classification.

2. Methods

2.1. Data and Meta-Data Acquisition

We augmented tissue, sex and age based on human sRNA-seq expression profiles. We used sRNA-Seq data from the SEA (Rahman et al., 2017) that contains 4243 samples and annotations in 350 datasets. The relatively large number of high-quality samples allowed us to use DL for data augmentation. Each sample contained annotations, sRNA expression counts of approximately 35000 sRNAs and expression information of potentially viral and bacterial transcripts (approximately 5600 'contaminants'), according to the output of the OASIS 2 sRNA analysis application (Rahman et al., 2018). Tissue prediction was based on sRNA expression profiles only, because the use of contamination profiles did not noticeably increase the accuracy of prediction; for age and sex prediction, contamination profiles were used. The number of datasets and samples is summarized in Table 1.

To avoid small classes with specific tissues we merged the available tissues using BTO in the SEA (Table 2) according to Fiosina et al. (Fiosina et al., 2019).

Age is a continuous variable and its exact prediction is a regression problem that might be highly inaccurate when solely based on sRNA expression information. To use the same methods as those used for the prediction of other annotation fields, we grouped ages into k intervals, $k = 2, 3, 4$. Table 3 summarizes the intervals used for age prediction.

2.2. Data scaling and filtering

Data scaling and filtering is described in detail in (Fiosina et al., 2019). In brief, the counts were normalized using RPM, each factor was normalized using a MinMax Scaler, the factors containing more than 30% zeros were removed (leaving approximately 2500 sRNAs and 2000 contaminants). Small groups were also removed, leaving 105 datasets for the analysis (see Table 1). We observed 23% cell lines and 77% tissue samples in our data. Fig. 1 illustrates the t-SNE plot for the tissue groups after the sample filtering.

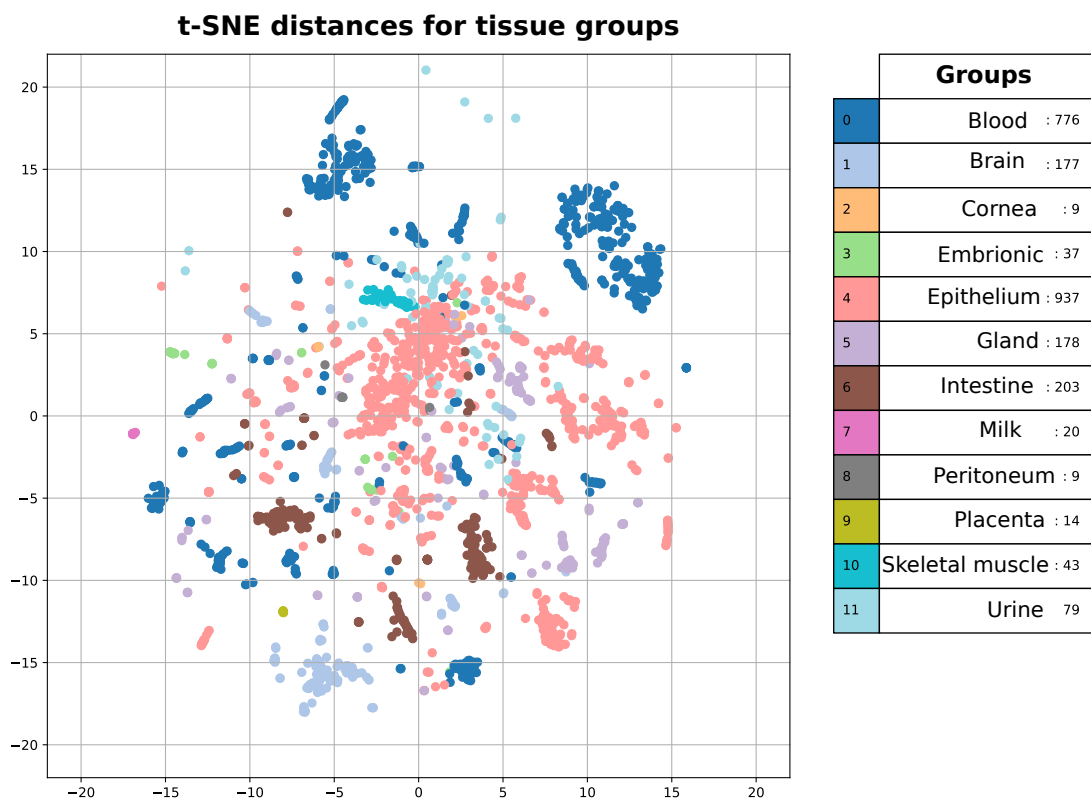


Figure 1: t-SNE Plot for available tissue types.

2.3. Models

2.3.1. DL model

We used a fully connected neuronal network (NN) architecture. It comprised one input layer with the number of inputs equal to the number of variables after the initial filtering. The NN contained three hidden layers with 1000, 250, and 250 neurons and drop-out rates of 0.5, 0.4, and 0.4, respectively (achieved by a grid search). The number of neurons in the output layer was equal to the number of predicted classes. The output data (the annotation classes) was encoded with integers $(0, 1, 2, \dots, num_of_classes)$, and transformed to categorical variables consisting of zeros and ones. We used the ReLU function to activate the input and the hidden layers, and the softmax function for the output layer, for a multi-class classification. As a loss function, either a binary or categorical cross-entropy was used. For the NN training, Adam optimizer was used. The NN was trained for 50 epochs with a batch size of 30.

2.3.2. RF model

We used a two-stage classification strategy. First, we used all features (remained after filtering) for the classification and feature importance calculation. We used the top-1000 features rated by their Gini index for the second stage classification with an increased number of trees (500 instead of 100). The mtry parameter was equal to the square root of the number of features. Given that the performance of RF method can be strongly affected by class imbalance, we down-sampled large classes to the size of the smaller ones.

2.3.3. Validation:

We implemented two types of cross-validation (CV) to investigate the accuracy of the data augmentation. First, we used the average accuracy of 5-fold CV. In this scenario, the training cells and test samples were randomly selected a priori, so that in most cases, samples from each dataset (experiment) could be included in the training and test sets.

Then, we performed "one-dataset-out" classifications, where specific datasets were removed from the training set and incorporated into the test set after ensuring that the respective tissues still remained in the training data set.

Throughout this manuscript, we refer to the 5-fold CV as "cross validation" and the validation for unseen datasets as "one dataset out".

2.3.4. Deep Lift:

To biologically trace the decisions of the DL model to the input features, we used DeepLIFT scores. DeepLIFT (Shrikumar et al., 2017) is an approach to assign importance scores, which demonstrate how important the value of each particular input is for each particular output. The scores are assigned according to the difference between a given input and some reference (neutral) input. The DeepLIFT method overperforms other scoring methods (Shrikumar et al., 2017); thus, it was selected for our analysis. The DeepLIFT method calculates scores by backpropagating the contributions of all neurons in the network to every feature of the input. Consequently, for each sample i , each input neuron j , and each output neuron k , a score $C_{i,j,k}$ is calculated, which represents an importance of an input j for an output k in the i -th input sample.

We have provided a three-step explanation of our augmentation models.

Firstly, we used a heatmap to visualize the DeepLIFT scores of an individual sample. This enabled us to understand, which sRNAs are important for a particular prediction.

Secondly, we analyzed important sRNAs for each class k . We selected samples, which belonged to the class k : $y_i = k$ and calculated the average difference scores for the correct class and other classes:

$$D1_{j,k} = \text{avg}_{y_i=k}(C_{i,j,k} - \text{avg}_{k' \neq k} C_{i,j,k'})$$

Then, we selected the top N sRNAs j according to $D1_{j,k}$ for each class k .

Finally, we investigated the number of sRNAs to be removed (to set their expression to zero), to change the classification results. For each sample i of class $y_i = k$ and each class $k' \neq k$, we calculated the score differences

$$D2_{i,j,k'} = C_{i,j,y_i} - C_{i,j,k'}.$$

We ordered the differences $D2(i, j, k')$ and set the expression of sRNAs $j = 0$. We stop the process when the classification changes from k to k' (similarity analysis) or to any other class $k'' \neq k$ (stability analysis). The corresponding average number of steps was applied to a matrix, which demonstrated "stability" of class (or "class similarity"). As a reference input, we used a vector of zeros.

2.3.5. Software libraries:

All the scripts for DL classification are developed in R based on the "keras" library. The RF models are also implemented in R, using the "randomForest" library. For quality metrics, we used R "caret" package. We used the Python 3.5 "sklearn.manifold" t-SNE library to build the t-SNE plots. DeepLIFT was implemented using the "deeplift" Python library version 0.6.9.0.

3. Results

3.1. Tissue prediction

3.1.1. Tissue group prediction:

We aimed to predict the tissue class, i.e., grouped tissue (2). Although grouping leads to a smaller number of classes, it increases the samples per class. This should reduce the problems due to class imbalances and the over-fitting of very small training classes. The prediction was based on sRNA expression profiles only.

CV experiments. In order to compare the performance of the DL and the RF models for datasets with a different degree of imbalance, we excluded classes for which less than 9 or 15 samples were available. Fig. 2 shows that the RF model is less accurate, particularly for the threshold of 9 (DL: 97%, RF: 85%). For the threshold of 15, the accuracy increases, however it is still significantly inferior to that of the DL models (DL: 98%, RF: 92%). We surmised that the better performance of the DL model, together with the fact that the accuracy is only slightly affected by the minimum class size, can be attributed to its resilience to class imbalances (Fig. 3 and 4).

"One dataset out" experiments. As detailed in the methods section, the aggregation of samples revealed 6 tissues with more than one dataset per tissue (see (Fiosina et al., 2019), Sample Filtering). For the "one dataset out" classification, one dataset was removed from the training set and was only used for testing the classification accuracy, as can be observed from the last two columns of 2. This resembles a real augmentation scenario in which a dataset with an unknown bias is augmented by the ML algorithm. Although the datasets

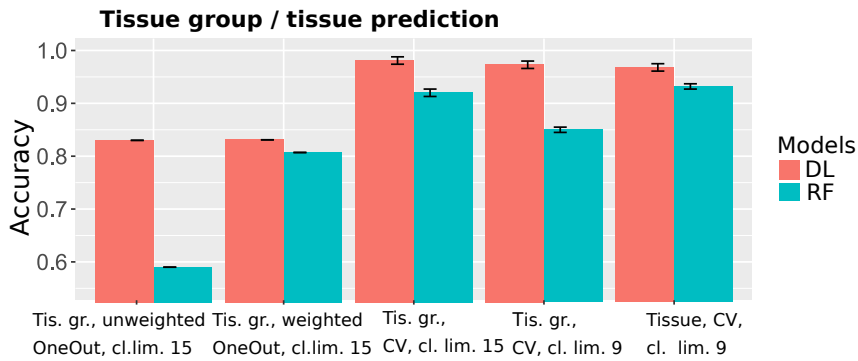


Figure 2: CV and 'one dataset out' accuracy of tissues and tissue-groups

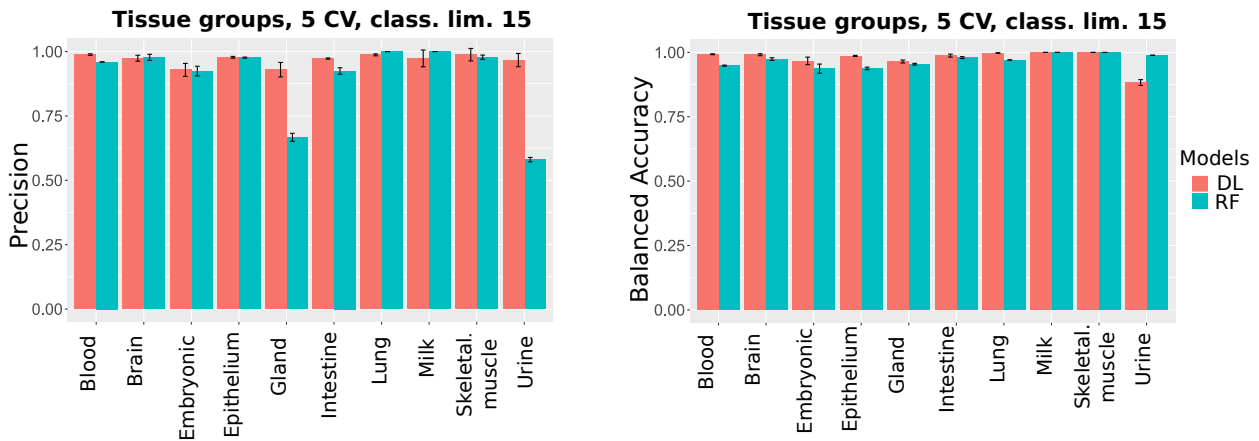


Figure 3: CV precision and accuracy for classes with min. 15 samples

in the training and testing sets were derived from the same tissue, they, most probably, possessed very distinct biases that could have originate from varying library preparation methods, the biological conditions of the samples, cell types, and diseases. The average accuracy of each group detection was 83.1% (DL) and 80.7% (RF) according to Fig. 5.

3.2. sRNA-seq sex prediction

For the determination of sex, we opted for enlarging the data set with contamination expression counts. Effectively, we tried to predict sex with six different model: using sRNA expression counts, using contaminants, using both, each for the RF and the DL algorithm (Fig.6). The best models were the DL and RF models based on both sRNAs and contaminations, with an accuracy of 77% and 76.9%, respectively. The other three models RF(RNA), DL(contaminations), and DL(sRNAs) demonstrated an accuracy of approximately 76.2%. It was unexpected that the model based only on contaminations predicted the sex with an accuracy of approximately 76% for both DL and RF models. Thus, for sex prediction, the DL model outperformed the RF model slightly.

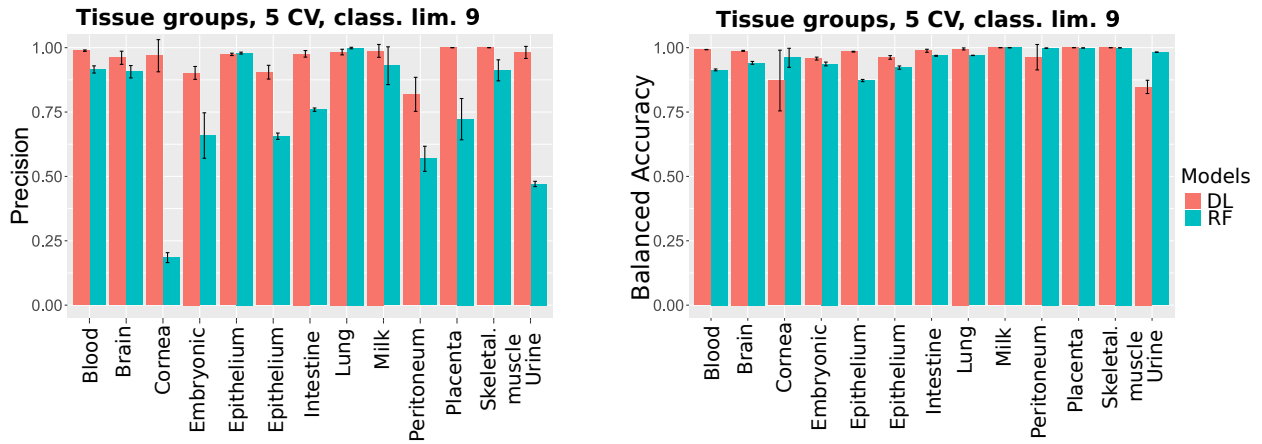


Figure 4: CV precision and accuracy for classes with min. 15 samples

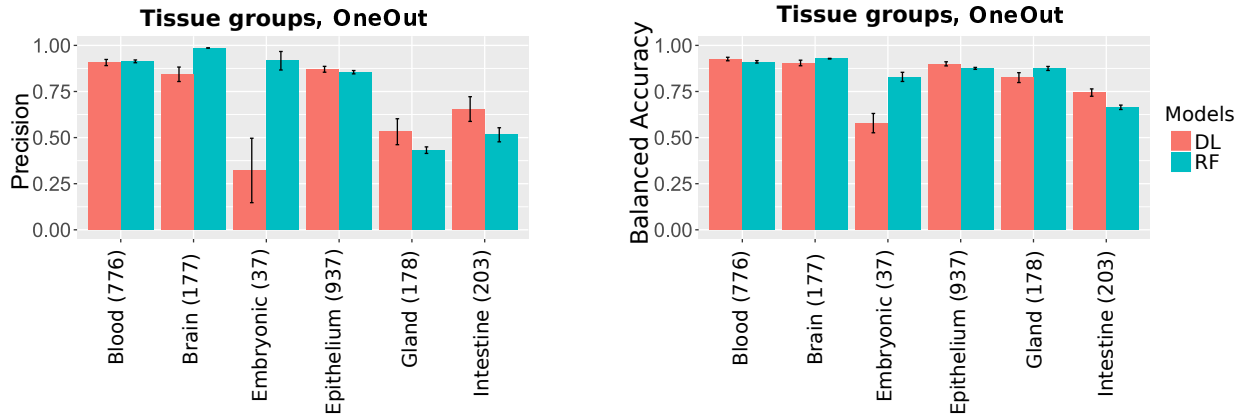


Figure 5: "One dataset out" tissue group prediction precision (left) and accuracy (right)

3.3. sRNA-seq age prediction

For predicting the age, we used the contamination expression counts similar to sex prediction. We predicted the age categories for three different splits yielding 2 and 4 categories, see Table 3. The results are presented in Fig. 6 and 7.

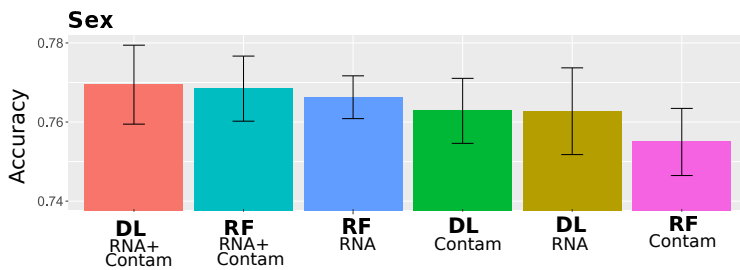


Figure 6: CV sex prediction accuracy with different models

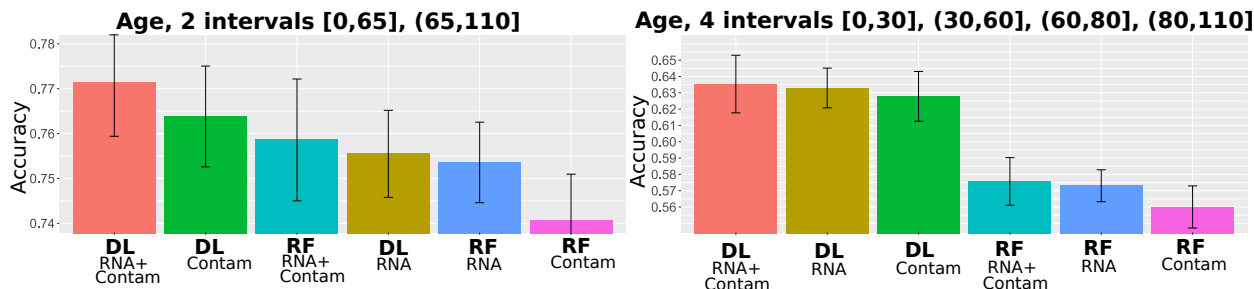


Figure 7: CV age prediction accuracy with different models

A comparison of results using 2 and 4 categories demonstrates that accuracy decreases with increasing number of age categories for all models. In both cases, the DL models slightly outperform the RF model, in particular for a split into 4 intervals. Combined sRNA and contaminant data for a DL model yielded the highest accuracy, i.e. 77.1% for a binary output and 63.5% for 4 intervals. Notably, DL using less data (sRNA or contaminant data only) presents an accuracy of 76.4% for binary output and 63.2% for 4 intervals. The RF models performed slightly worse on average with a maximum accuracy 75.8% for binary output and 4 intervals and 57.5% for 4 intervals.

3.4. Explanation of deep learning results

DL-based models are called "black boxes" because it is often unclear how the models arrive at their decisions. However, particularly in biological and medical settings, it is important to understand what enables algorithms to classify a sample, as the feature may be related to a cause as well as to a possible treatment. We investigated the explainability of automatic metadata augmentation with DL models, using backpropagation with the DeepLIFT method.

3.4.1. Prediction explanation for individual samples

To visualize the backpropagation results, we used heatmaps that represented the scores for each individual class (Fig. 8, 9 and 10).

The figures demonstrate that the visual representations of DeepLIFT scores may explain the factors important for a particular output of the NN. This shows that deep neural networks can indeed offer explainable and interpretable results.

3.4.2. Average scores for sample prediction and enrichment

The most important sRNAs for a class can, however, not be determined on a per-sample basis as individual samples show rather large variations. Thus, we computed $D1_{j,k}$ for each tissue k as outlined in 2.3.4. Using these scores, we selected the top $N = 300$ sRNAs j and calculated the average expression for each class (Fig 11).

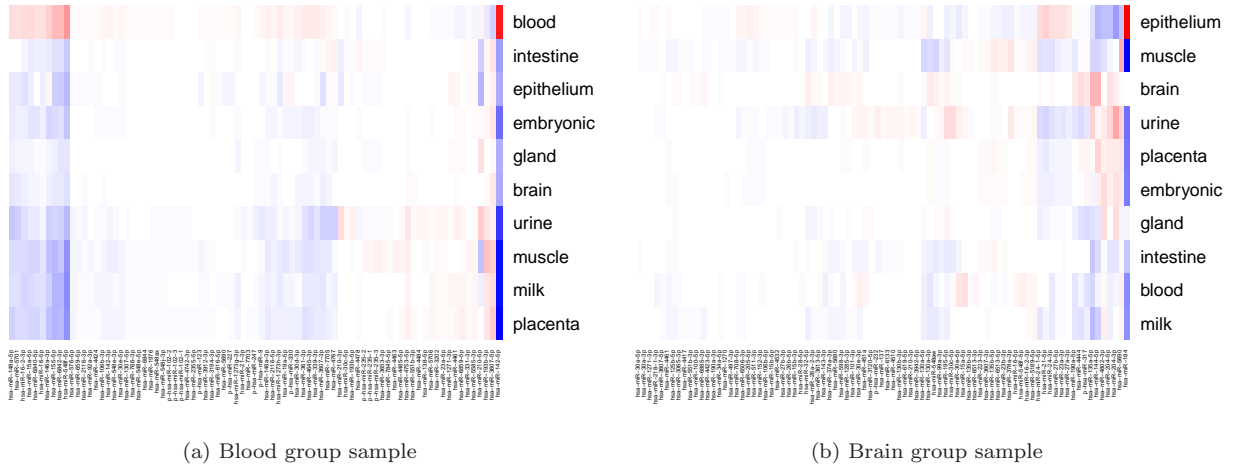


Figure 8: DeepLIFT scores for tissue group classification. On the left, we see some sRNAs clearly voting for the blood group (one sRNA on the right, and a cluster on the left). Particular sRNAs vote against the blood group (second and third on the left). Similarly, other tissues have specific sRNAs the score for or against the tissue.

We observed that factors with big average DeepLIFT scores do not show a clear separation by expression levels. We still see some clusters of sRNAs, which are characteristic for the groups. These observations may be explained by non-linear class separation of the DL, which is not reflected just by average expression per class.

To make sure that the results contain biologically relevant sRNAs, we investigated the enrichment of biological categories based on important sRNAs. We used the model based on miRNA only, as the enrichment information is available mostly for miRNAs (Fig. 12 and Table 4).

Our enrichment analysis clearly shows an overrepresentation of biologically meaningful sRNAs for a given target tissue, demonstrating that DeepLIFT scores allow the extraction of important tissue-specific sRNAs. We conclude that DeepLIFT is a viable method to explain DL decisions for genomic data.

3.4.3. Stability of Solution

Further, we wanted to assess if DeepLIFT scores could provide insights into the stability of DL models. We ordered the differences $D2_{i,j,k'}$ and calculated the number of steps to change the predicted class according to 2.3.4 and (13). Note that some classes are stable, other classes are quite unstable. These results most probably reflect the specificity and quantity of group-specific feature expressions.

4. Conclusion and future work

Depending on the outcome variable (e.g. tissue, sex, age) automatic metadata augmentation can be a good option to annotate the missing metadata using sRNA expressions. The DL-based classification

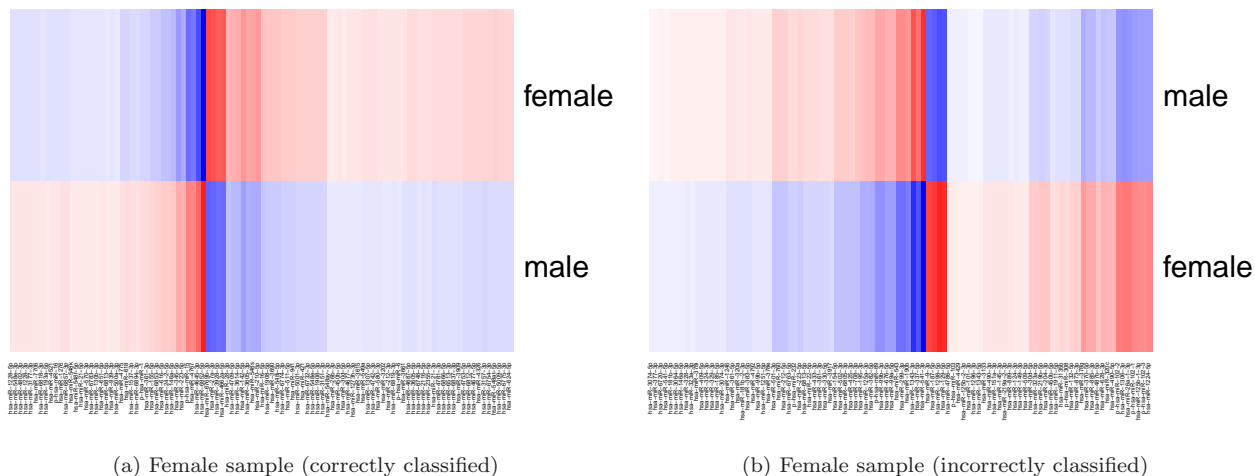


Figure 9: DeepLIFT scores for sex classification. For both samples, we see a number of sRNAs voting for and against each class. Both are classified as female. On the left, there is a majority of sRNAs voting for female.

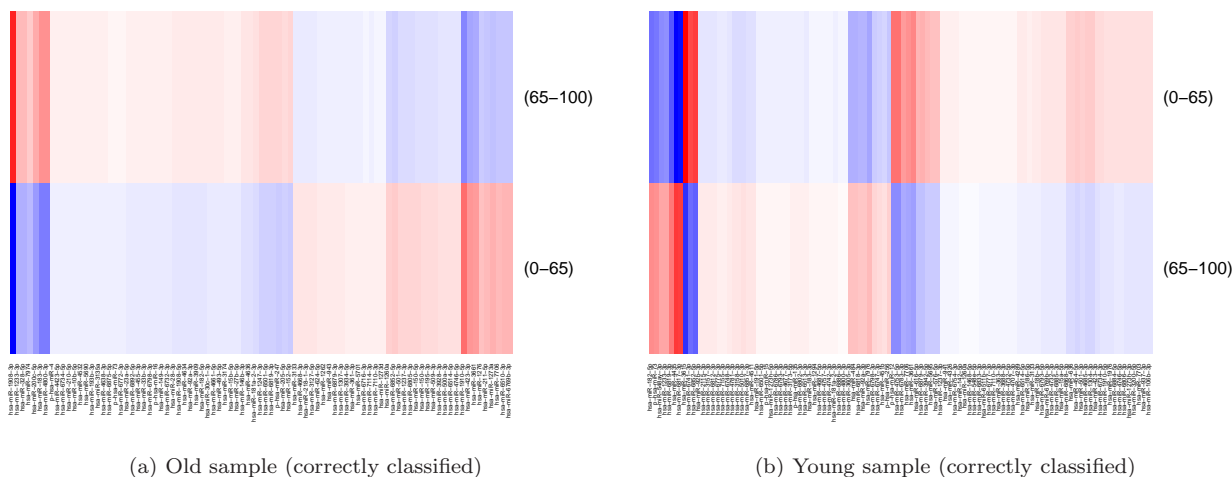


Figure 10: DeepLIFT scores for age classification. For both samples, we see a number of sRNAs voting for and against each class. However, the left sample has more sRNAs which vote for the old class and the right sample has more sRNAs that strongly vote for the young class.

accuracy of tissue and sex predictions reaches 98% and 77%, respectively, the classification of age groups (or the regression of age) seems to demonstrate an inferior performance. In general, metadata augmentation, as undertaken in this study is dependent on the occurrence of the tissue of interest, or a similar tissue, in the training dataset of the classifier. Another general problem is that of class imbalances and very rare classes. In this work, we have used an ontology-based grouping of rare classes to higher ontological nodes to increase the sample number for a given class. In future work, we plan to use a hierarchical classification, from general to specific tissue classes, to investigate the classification performance across the ontological hierarchy. We

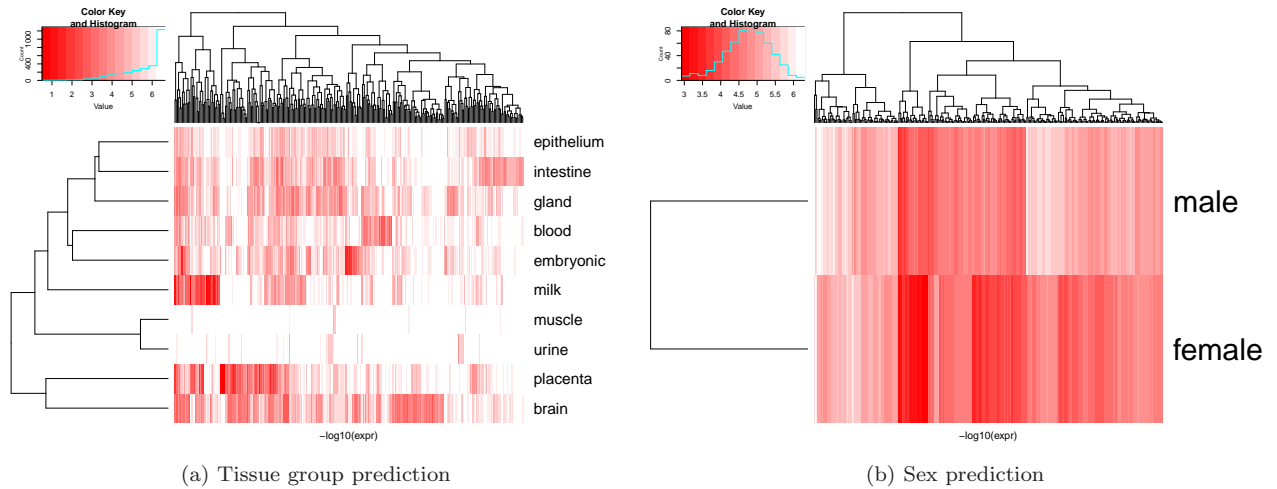


Figure 11: Expression of sRNAs with top 300 DeepLIFT scores.

have also demonstrated that, in general, the inclusion of contamination profiles in classification models improves the accuracy for sex and age.

sRNA expression profiles seem to be suitable for the augmentation of tissue information. A CV-based tissue group classification achieves an accuracy over 98%. In the "one dataset out" scenario, with a specific data set with a specific bias missing from the training data, samples from the unseen dataset are classified with an accuracy of approximately 80%.

For sex classification, the DL model achieved an accuracy of about 77%, which may not be sufficient for accurate sex classification. This relatively low accuracy indicates that there may be no sex-specific expressed sRNAs for the X- or Y-chromosomes. Similarly, we obtained an accuracy of 77% for predicting whether a person is younger or older than 65. For a split into 4 intervals, accuracy decreased to 64%, indicating that the sRNA transcriptome does not consistently change with .

Lastly, we demonstrated that DL models can be explained both for individual samples and on average. For this purpose, the DeepLIFT scores demonstrated very promising results.

Acknowledgments

We would like to thank Daniel Sumner Magruder and Hannes Wartmann for helpful and essential suggestions. The research was supported by the German Federal Ministry of Education and Research (BMBF), project Integrative Data Semantics for Neurodegenerative research (031L0029); by German Research Foundation (DFG), project Quantitative Synaptology (SFB 1286 Z2) and by Volkswagen Foundation.

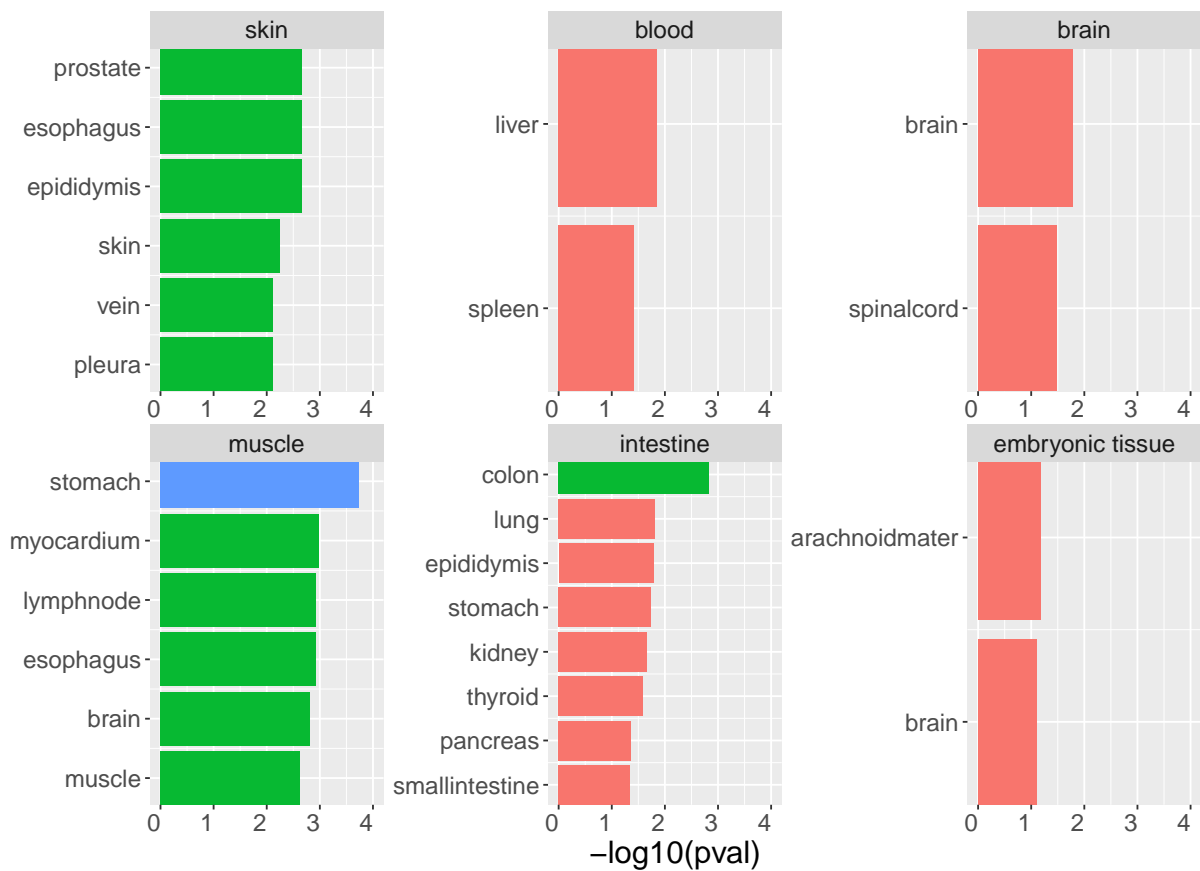


Figure 12: Tissue enrichment. We see enrichment in 6 categories. For most of them, we see enrichment of tissue-relevant terms. For example, for epithelium we see skin, vein and pleura categories, for blood - liver and spleen, which are blood producing organs; for brain - brain and spinal cord, which are central nervous system relevant.

References

References

- Bach, S., Binder, A., et al. (2015). On pixel-wise explanations for non-linear classifier decisions by layer-wise relevance propagation. *PLoS ONE*, 10(7).
- Breiman, L. (2001). Random forests. *Machine Learning*, 45(1):5–32.
- Buckberry, S., Bent, S. J., Bianco-Miotto, T., and Roberts, C. (2014). massir: a method for predicting the sex of samples in gene expression microarray datasets. *Bioinformatics*, 30:2084–2085.
- Choi, E., Bahadori, M., et al. (2016). Retain: An interpretable predictive model for healthcare using reverse time attention mechanism. In Lee, D. D., Sugiyama, M., Luxburg, U. V., Guyon, I., and Garnett, R., editors, *Advances in Neural Information Processing Systems 29*, pages 3504–3512. Curran Associates, Inc.
- Ellis, S. et al. (2018). Improving the value of public rna-seq expression data by phenotype prediction. *Nucleic Acids Res.*, 46(9).
- Fiosina, J., Fiosins, M., and Bonn, S. (2019). Deep learning and random forest-based augmentation of srna expression profiles.

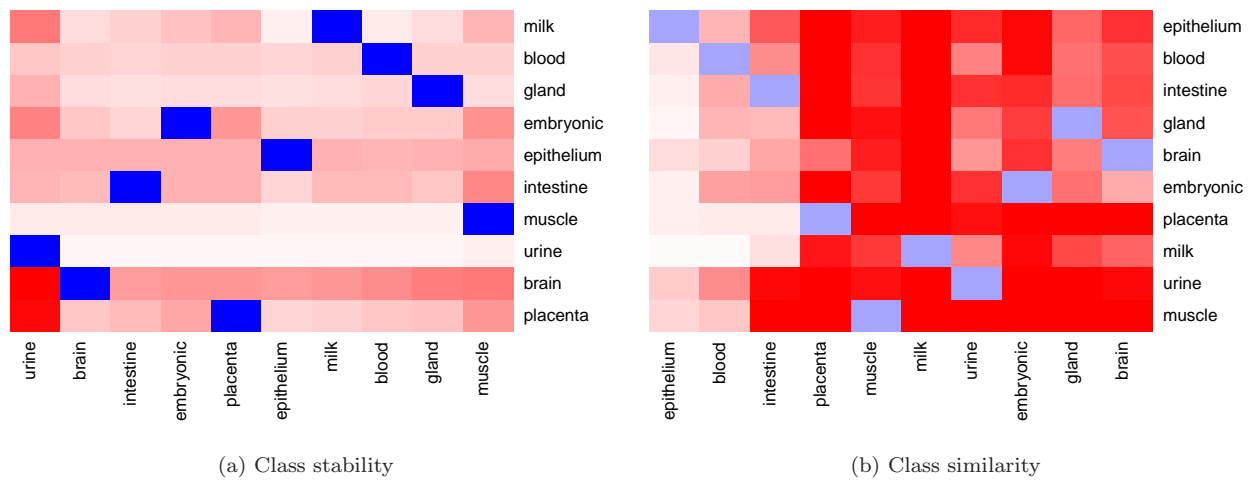


Figure 13: Stability and similarity of classes for tissue group classification. Intensity of red color shows number of steps to change class. Some classes are stable, such as the brain, intestine, and epithelium. Other classes like the urine, skeletal muscle, or gland are quite unstable and are easily transformed to the epithelium or blood groups.

In Cai, Z., Skums, P., and Li, M., editors, *Bioinformatics Research and Applications*, pages 159–170. Springer International Publishing.

GEO. Gene Expression Omnibus. <https://www.ncbi.nlm.nih.gov/geo/>.

Guo, L. et al. (2017). mirna and mrna expression analysis reveals potential sex-biased mirna expression. *Scientific Reports*, 7.

Hadley, D., Pan, J., et al. (2017). Precision annotation of digital samples in ncbis gene expression omnibus. *Sci. Data*, 4:170125.

Johnson, N., Dhroso, A., Hughes, K., and Korkein, D. (2018). Biological classification with rna-seq data: Can alternatively spliced transcript expression enhance machine learning classifiers? *RNA*, 24:1119–1132.

Kong, Y. and Yu, T. (2018). A deep neural network model using random forest to extract feature representation for gene expression data classification. *Scientific Reports*, 8.

Lakkaraju, H., Kamar, E., Caruana, R., and Leskovec, J. (2017). Interpretable & explorable approximations of black box models. *CoRR*, abs/1707.01154.

LeCun, Y., Bengio, Y., and Hinton, G. (2015). Deep learning. *Nature*, 521.

Li, Y. et al. (2019). Deep learning in bioinformatics: introduction, application, and perspective in big data era. *bioRxiv*.

Madan, S., Fiosins, M., et al. (2018). A semantic data integration methodology for translational neurodegenerative disease research. *figshare*.

Molnar, C. (2019). *Interpretable Machine Learning. A Guide for Making Black Box Models Explainable*. Lulu.

Montavon, G., Lapuschkin, S., et al. (2017). On pixel-wise explanations for non-linear classifier decisions by layer-wise relevance propagation. *Pattern Recognition*, 65:211–222.

O'Brien, R. and Ishwaran, H. (2019). A random forests quantile classifier for class imbalanced data. *Pattern Recognition*, 90:232–249.

Rahman, R.-U. et al. (2018). Oasis 2: improved online analysis of small rna-seq data. *BMC Bioinformatics*, 19(54).

Rahman, R.-U., Sattar, A., Fiosins, M., et al. (2017). Sea: The small rna expression atlas. *bioRxiv*.

Ribeiro, M. T., Singh, S., and Guestrin, C. (2016). "why should i trust you?": Explaining the predictions of any classifier. In *Proceedings of the 22Nd ACM SIGKDD International Conference on Knowledge Discovery and Data Mining*, KDD '16, pages 1135–1144, New York, NY, USA. ACM.

- Robnik-ikonja, M. and Bohanec, M. (2018). Perturbation-based explanations of prediction models. In J., Z. and F., C., editors, *Human and Machine Learning. HumanComputer Interaction Series*. Springer, Cham.
- Shrikumar, A., Greenside, P., and Kundaje, A. (2017). Learning important features through propagating activation differences. In *Proceedings of the 34th International Conference on Machine Learning, ICML 2017, Sydney, NSW, Australia, 6-11 August 2017*, pages 3145–3153.
- Statnikov, A., Wang, L., and Aliferis, C. F. (2008). A comprehensive comparison of random forests and support vector machines for microarray-based cancer classification. *BMC Bioinformatics*, 9.
- Storz, G. (2002). An expanding universe of noncoding rnas. *Science*, 296(5571):1260–1263.
- Webb, S. (2018). Deep learning for biology. *Nature*, 554:555–557.
- Wilkinson, M. D. et al. (2016). The fair guiding principles for scientific data management and stewardship. *Sci. Data*, 3:160018.
- Xiao, T. et al. (2015). Learning from massive noisy labeled data for image classification. In *2015 IEEE Conf. on Comp. Vision and Pattern Recognition (CVPR)*, pages 2691–2699.

Table 1: Number of samples and datasets used to augment tissue, age and sex. The samples comprised 42% males and 58% females.

Metadata field	No. Datasets	No. Samples
Tissue	128	2806
Tissue after filtering	105	2215
Sex	41	1591
Age	27	888

Table 2: Tissue and cell line grouping according to ontologies.

Tissue group	Contained tissues
blood_group	blood, blood plasma, blood serum, peripheral blood, umbilical cord blood, serum, buffy coat, immortal human B cell, liver, lymphoblastoid cell
brain_group	brain, cingulate gyrus, motor cortex, prefrontal cortex, neocortex
epithelium_group	skin, dermis, epidermis, breast, oral mucosa, larynx
gland_group	prostate gland, testis, kidney, bladder, uterine endometrium, tonsil, lymph node
intestine_group	intestine, colon, ileal mucosa

Table 3: Age intervals used in prediction.

2 intervals	3 intervals	4 intervals
[0;65],(65;110]	[0;45],(45;70],(70;110]	[0;30],(30;60],(60;80],(80;110]

Table 4: Enriched miRNAs for tissue prediction

Category	enriched miRNAs
skin	hsa-miR-205-5p; hsa-miR-205-3p; hsa-miR-193a-5p; hsa-miR-23a-3p; hsa-miR-21-5p; hsa-miR-3195; hsa-miR-27a-3p; hsa-miR-224-5p; hsa-miR-98-5p; hsa-miR-944
blood	hsa-miR-99a-5p; hsa-miR-142-5p; hsa-miR-4732-3p; hsa-miR-486-5p; hsa-miR-15a-5p; hsa-miR-1976; hsa-miR-16-5p; hsa-miR-16-2-3p; hsa-miR-129-5p; hsa-miR-1224-5p
brain	hsa-miR-153-3p; hsa-miR-138-5p; hsa-miR-100-5p; hsa-miR-9-5p; hsa-miR-874-3p; hsa-miR-124-3p; hsa-miR-125b-5p; hsa-miR-181c-3p; hsa-miR-654-3p; hsa-miR-598-3p
muscle	hsa-miR-378a-5p; hsa-miR-133a-3p; hsa-miR-193b-3p; hsa-miR-4463; hsa-miR-6723-5p; hsa-miR-4644; hsa-miR-1271-5p; hsa-miR-378a-3p; hsa-miR-4485-3p; hsa-miR-193b-5p
intestine	hsa-miR-215-5p; hsa-miR-194-3p; hsa-miR-194-5p; hsa-miR-192-3p; hsa-miR-192-5p; hsa-miR-200b-3p; hsa-miR-200b-5p; hsa-miR-19b-3p; hsa-miR-31-5p; hsa-miR-200c-3p
embryonic tissue	hsa-miR-92b-3p; hsa-miR-18b-3p; hsa-miR-363-3p; hsa-miR-421; hsa-miR-3195; hsa-miR-335-3p; hsa-miR-887-3p; hsa-miR-3648; hsa-miR-4417; hsa-miR-130b-3p

Table 5: Enriched miRNAs for tissue prediction

Classification model	Class 1	Class 2	No. of steps Class1 into Class2	No. of steps Class2 into Class1
Sex prediction	female	male	15.9	13.7
Age prediction	[0-65]	(65-110]	8.6	15.0